*Solar Energy* Vol. 26, pp. 297–306, 1981
Printed in Great Britain. 

0038-092X/81/040297-10$02.00/0


# NONLINEAR DYNAMIC MODEL OF A SOLAR STEAM GENERATOR

ASOK RAY†
Control and Flight Dynamics Division, The C.S. Draper Laboratory, Inc., Cambridge, MA 02139, U.S.A.

(*Received* 29 *April* 1980; *accepted* 9 *September* 1980)

**Abstract**—A thermal-hydraulic model of a once-through subcritical steam generator has been developed for predicting dynamic characteristics of solar thermal power plants as well as for control system design. The purpose of the model is to evaluate the overall system performance and component interaction with sufficient accuracy for controller design, rather than to describe the microscopic details occurring within the steam generator.

The three-section (compressed water, two-phase mixture, and superheated steam) model with time-varying phase boundaries is described by a set of nonlinear differential equations derived from conservation of mass, momentum and energy. Local stability of the model has been examined at different levels of insolation. Transient response of six plant variables due to independent step disturbances in three input variables are presented as typical results.

## INTRODUCTION

Recently, much attention has been paid to central solar receivers for application to commercial scale steam–electric power generation systems. The types of steam generators being considered are: once-through, natural recirculation and forced recirculation[1]. Although some manufacturers view that forced circulation drum-type units are the best choice for solar applications[1], the 10-MWe DOE solar thermal plant to be built at Barstow, CA, is designed to have a once-through subcritical steam generator with throttle conditions at 510°C, $1.01 \times 10^7$ N/m$^2$ (950°F, 1465 psia)[2].

The technology of solar thermal power generation is yet at an early development stage. Unlike fossil and nuclear steam power generation systems, solar thermal plants must undergo daily start-up and shutdown, and very frequent load changes due to variations in insolation. In addition, thermal hydraulic dynamics of once-through steam generators are complex; operating experience at fossil plants shows that once-through steam generators are relatively more difficult to control[3]. Design and development of commercial scale solar thermal plants cannot be accomplished by simple modification of existing fossil and nuclear plant parameters; *a priori* analytical studies are essential. Mathematical modeling and simulation have been proved to be useful and analytical tools for investigation of potential operational and control problems in large scale industrial processes as well as for control system design[4]. Their application to solar thermal plants is very timely.

This paper presents a nonlinear dynamic model of a once-through subcritical steam generator to be used as an element in overall system simulation and controller design of solar thermal plants. The model is not intended for studying microscopic thermal-hydraulic phenomena and flow maldistribution among the tubes. The modeling methodology is an extension of the earlier work of Ray and Bowman[5] dealing with gas-cooled nuclear power plants. After some minor modifications, the methodology of Ref.[5] was successfully applied to model a 386-MWe oil-fired once-through subcritical unit; with the aid of the model, a controller was designed and implemented in the real plant resulting in improved performance[3].

The model equations are arranged in state-space form to facilitate digital simulation and control system design. Steady-state solutions of the model equations were obtained at different levels of insolation from 100 to 40 per cent. The model was linearized around several equilibrium points, and small signal stability was examined. The nonlinear model was simulated in time domain, and transient responses of six plant variables for independent step disturbances in three different input variables are presented as typical results.

A summary of the equations that constitute the model is listed in the Appendix.

## SYSTEM DESCRIPTION

The central solar receiver under study transfers concentrated solar energy reflected from the mirrors of the heliostat assembly to the steam–electric power generation system. The receiver is built approximately in the shape of a cylinder of length 13 m (43 ft) and diameter 7.2 m (23.8 ft), mounted vertically on a tower about 74 m (243 ft) above the ground level[2, 6]. The heliostats (at the ground level) surround the receiver tower and direct the collected solar energy onto full 360° external surface of the receiver[7].

The (nearly) cylindrical surface of the receiver is fabricated by 24 water/steam cooled flat vertical panels—6 preheater panels and 18 steam generator panels. Each panel consists of 73 straight vertical tubes (made of alloy steel) which are welded together. The preheater panels receive pressurized water from the feed pump, and discharge into a common manifold that delivers warm subcooled water into the steam generator panels. Superheated steam from the steam generators flows into the steam header for delivery to the turbine-generator and/or thermal storage system depending on the operational mode of the solar plant. For the operational mode

†This work was done while the author was at Carneigie-Mellon University, Pittsburgh, PA.

under study, there is no flow to the thermal storage system.

## MODELING APPROACH

The purpose of the model is to evaluate overall system performance and component interaction with sufficient accuracy for controller design, rather than to describe microscopic details occurring within the steam generator. In this perspective, several assumptions have been made to simplify the model. If the model is a detailed description of the process, computer runs for system simulation would be costly, and the task of controller design too complicated.

The physical process of steam generation consists of distributed parameter dynamic elements, mathematically represented by nonlinear partial differential equations with space and time as independent variables. A lumped parameter approximation was used to formulate a finite-dimensional state-space model. Partial differential equations were reduced to a finite number of ordinary differential equations with time as the independent variable. This approach has been shown to be adaquate in modeling other steam power generation systems by experimental verification [8–11].

Model equations were formulated from: Fundamental equations of mass, momentum, and energy conservation; semi-empirical relationships for fluid flow and heat transfer; and state relations for thermodynamic properties of water/steam.

†Transport delay means the time required by a fluid particle to flow through a given distance.

The steam generator model was developed for normal operating conditions; however, the model can be extended to investigate start-up and shutdown operations without changing the basic structure.

### *Assumptions*

Major assumptions in addition to lumped parameter approximation are:

(1) Uniform fluid flow over pipe cross sections.

(2) Identical flow through each steam generator tube.

(3) Uniform incidence of solar flux on steam generator tube surface from heliostats.

(4) Choked flow of steam through the turbine valve.

The following parameters were evaluated and found to be negligible:

(1) Axial conduction of heat in tube wall and water/steam.

(2) Transport delay† due to water/steam flow in steam generator tube.

(3) Velocity head of water/steam in each section of steam generator tube.

## DEVELOPMENT OF MODEL EQUATIONS

A typical tube of the once-through subcritical steam generator has been modelled in three sections, i.e. compressed water (economizer), wet steam (evaporator), and superheated steam (superheater), as shown in Fig. 1. The length of each section is allowed to vary with time, and fluid properties at the phase boundaries are, therefore, time-varying. The model equations are developed using control volumes with time-varying control surfaces as

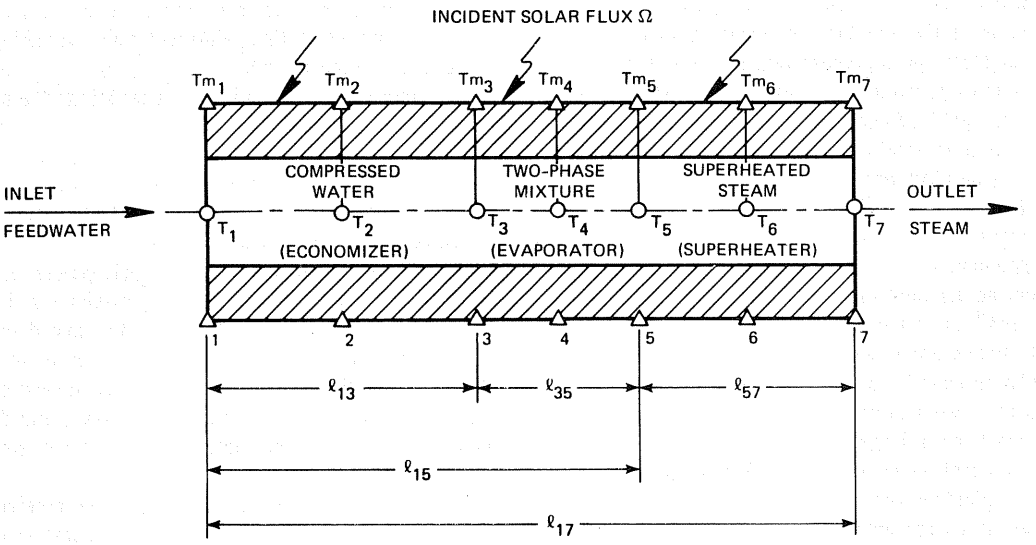


LEGEND

NODE 1 – FEEDWATER ENTRY
NODE 2 – AVERAGE POINT FOR ECONOMIZER
NODE 3 – ECONOMIZER/EVAPORATOR BOUNDARY
NODE 4 – AVERAGE POINT FOR EVAPORATOR
NODE 5 – EVAPORATOR/SUPERHEATER BOUNDARY
NODE 6 – AVERAGE POINT FOR SUPERHEATER
NODE 7 – SUPERHEATER OUTLET

Δ – NODES FOR TUBE METAL
○ – NODES FOR SECONDARY COOLANT
Tm – TUBE WALL TEMPERATURE
T – WATER/STEAM TEMPERATURE

NOTES: 1. NODES 2, 3, 4, 5, AND 6 ARE TIME-VARYING; NODES 1 AND 7 ARE FIXED.
2. $\ell_{17}$ = STEAM GENERATOR TUBE LENGTH; $\ell_{17} = \ell_{15} + \ell_{57} = \ell_{13} + \ell_{35} + \ell_{57}$

Fig. 1. Schematic view of a steam generator tube with time-varying phase boundaries.

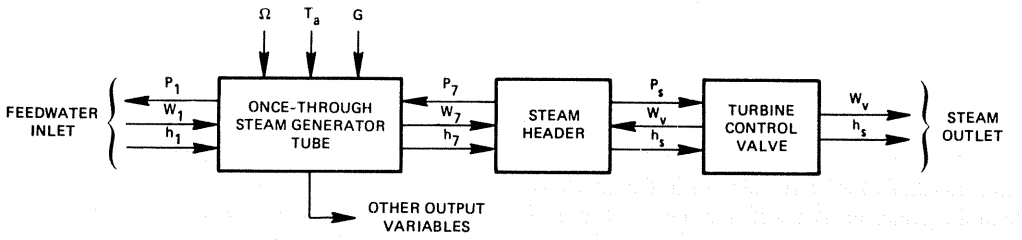


NOTE: ARROWS ENTERING A MODEL – INPUT VARIABLES
ARROWS LEAVING A MODEL – OUTPUT VARIABLES
SYMBOLS ARE DEFINED IN NOMENCLATURE

Fig. 2. Model solution diagram.

shown in Fig. 1. A model solution diagram indicating the input and output variables is given in Fig. 2.

*Water/steam flow*

A study of temporal acceleration in the momentum equations in each section revealed very fast decaying transients due to low inertia of steam/water path. The control system and the process external to the steam generator behave as low pass filters with respect to these fast transients. Hence, these transients have little bearing on the design of control systems. Since the volume of the steam generator tube ensemble is small in comparison to the steam header feeding the thermal storage system and turbine, water/steam flow through each section of the tube is assumed incompressible, and flow through the steam header as compressible. Therefore, temporal acceleration and compressibility terms inside the steam generator tube have been omitted. Steady-state calculations show that pressure drop due to frictional, gravational and velocity effects across the economizer, evaporator and superheater are typically 830 N/m$^2$(1.20 psi), 4070 N/m$^2$ (5.8 psi), and 2900 N/m$^2$ (4.2 psi), respectively at the rated fluid flow. These pressure differences are not significant in comparison to the steam header pressure $1.01 \times 10^7$ N/m$^2$(1465 psia). To simplify the model, the pressures at the phase boundaries are derived from the steam header pressure as functions of water/steam flow and lengths of respective sections.

$$P_5 = P_7 + [K_{f6}(W_5/W^*)^2 + \lambda_5]l_{57} \tag{1}$$

$$P_3 = P_5 + [K_{f4}(W_3/W^*)^2 + \lambda_3]l_{35} \tag{2}$$

$$P_1 = P_3 + [K_{f2}(W_1/W^*)^2 + \lambda_1]l_{13} \tag{3}$$

where $W_7 = W_5 = W_3 = W_1$ because of the assumption that water/steam flow is incompressible inside the steam generator tube.

The conservation of mass and energy in the three time-varying control volumes (see Fig. 1) yield:

Economizer

$$\mathrm{d}(A_f\rho_2 l_{13})\,\mathrm{d}t = W_1 - W_3 + A_f\rho_3\,\mathrm{d}l_{13}/\mathrm{d}t \tag{4}$$

$$\mathrm{d}(A_f\rho_2 u_2 l_{13})\mathrm{d}t = W_1h_1 - W_3h_3 + Q_2 + A_f\rho_3h_3\,\mathrm{d}l_{13}/\mathrm{d}t. \tag{5}$$

Evaporator

$$\mathrm{d}(A_f\rho_4 l_{35})/\mathrm{d}t = W_3 - W_5 + A_f(\rho_5\,\mathrm{d}l_{15}/\mathrm{d}t - \rho_3\,\mathrm{d}l_{13}/\mathrm{d}t) \tag{6}$$

$$\mathrm{d}(A_f\rho_4 u_4 l_{35})\mathrm{d}t = W_3h_3 - W_5h_5 + Q_4 + A_f(\rho_5h_5\,\mathrm{d}l_{15}/\mathrm{d}t - \rho_3h_3\,\mathrm{d}l_{13}/\mathrm{d}t). \tag{7}$$

Superheater

$$\mathrm{d}(A_f\rho_6 l_{57})/\mathrm{d}t = W_5 - W_7 - A_f\rho_5\,\mathrm{d}l_{15}/\mathrm{d}t \tag{8}$$

$$\mathrm{d}(A_f\rho_6 u_6 l_{57})/\mathrm{d}t = W_5h_5 - W_7h_7 + Q_6 - A_f\rho_5h_5\,\mathrm{d}l_{15}/\mathrm{d}t \tag{9}$$

where

$$\mathrm{d}l_{15}/\mathrm{d}t = \mathrm{d}l_{13}/\mathrm{d}t + \mathrm{d}l_{35}/\mathrm{d}t = -\mathrm{d}l_{57}/\mathrm{d}t.$$

Since the spatial average temperature of water in economizer does not change appreciably with time, $\mathrm{d}u_2/\mathrm{d}t$ is assumed to be zero. Setting $W_3 = W_1$ eqns (4) and (5) yield

$$\mathrm{d}l_{13}/\mathrm{d}t = (W_1(h_1 - h_3) + Q_2)/(A_f\rho_3(u_2 - h_3)). \tag{10}$$

Similarly, for the evaporator, setting $\mathrm{d}u_4/\mathrm{d}t = 0$ and $W_5 = W_3 = W_1$, eqns (6) and (7) are simplified as

$$\mathrm{d}l_{15}/\mathrm{d}t = [W_1(h_3 - h_5) + Q_4 + A_f\rho_3(u_4 - h_3)\,\mathrm{d}l_{13}/\mathrm{d}t]/[A_f\rho_5(u_4 - h_5)]. \tag{11}$$

For the superheater, setting $W_7 = W_5 = W_1$, eqns (8) and (9) yield

$$\mathrm{d}u_6/\mathrm{d}t = [W_1(h_5 - h_7) + Q_6 + A_f\rho_5(u_6 - h_5)\,\mathrm{d}l_{15}/\mathrm{d}t]/(A_f\rho_6/l_{15}). \tag{12}$$

*Energy storage in tube wall*

Energy storage in the three sections of the thick tube wall is important for evaluation of thermal-hydraulic transients. Assuming external tube wall temperatures to be constant in the evaporator[12] and linear with respect to tube length in the economizer and superheater, wall temperatures at the section boundaries (see Fig. 1) are:

$$T_{m1} = 2T_{m4} - T_{m2} \tag{13}$$

$$T_{m3} = T_{m4} \quad (14)$$

$$T_{m5} = T_{m4} \quad (15)$$

$$T_{m7} = 2T_{m6} - T_{m4}. \quad (16)$$

Dynamic equations for energy storage in the time-varying control volumes in each section of tube wall are:

Economizer

$$\mathrm{d}(C_m l_{13} T_{m2})/\mathrm{d}t = Q_{m2} - Q_2 + C_m T_{m3}\, \mathrm{d}l_{13}/\mathrm{d}t. \quad (17)$$

Evaporator

$$\mathrm{d}(C_m l_{35} T_{m4})/\mathrm{d}t = Q_{m4} - Q_4 + C_m(T_{m5}\, \mathrm{d}l_{15}/\mathrm{d}t - T_{m3}\, \mathrm{d}l_{13}/\mathrm{d}t). \quad (18)$$

Superheater

$$\mathrm{d}(C_m l_{57} T_{m6})/\mathrm{d}t = Q_{m6} - Q_6 - C_m T_{m5}\, \mathrm{d}l_{15}/\mathrm{d}t. \quad (19)$$

Rearranging eqns (17)–(19) with eqns (13)–(16)

$$\mathrm{d}T_{m2}/\mathrm{d}t = (Q_{m2} - Q_2)/(C_m l_{13}) + [(T_{m4} - T_{m2})/l_{13}]\mathrm{d}l_{13}/\mathrm{d}t \quad (20)$$

$$\mathrm{d}T_{m4}/\mathrm{d}t = (Q_{m4} - Q_4)/(C_m l_{35}) \quad (21)$$

$$\mathrm{d}T_{m6}/\mathrm{d}t = (Q_{m6} - Q_6)/(C_m l_{57}) + [(T_{m6} - T_{m4})/l_{57}]\, \mathrm{d}l_{15}/\mathrm{d}t. \quad (22)$$

*Heat transfer*

Heat transfer at the external surface of a typical tube consists of incident solar energy from heliostat ensemble, and reradiation and convective losses from tube surface to the environment. A model of solar energy collector can be formulated on the basis of a specific heliostat ensemble[7]. In this study, uniform solar flux is assumed as an input to the steam generator (see Fig. 2). Surface areas per unit length of steam generator tube are taken as known parameters for incident solar energy, and reradiation and convection losses. Reradiation losses from a section of tube is obtained from the average of fourth power of absolute temperatures.

$$Q_r = \sigma \epsilon A_r l[(T_m + T_o)^4 - (T_a + T_o)^4]. \quad (23)$$

Convective loss from tube surface is due to both natural and forced convection. Heat transfer coefficient due to turbulent natural convection is proportional to $(\Delta T)^{0.33}$[13]. On the other hand, forced convective heat transfer is dependent on both magnitude and direction of air flow over the tube surface[13]. Air velocity $G$ over the tube surface is consisdered as a model input. Total convection losses are approximated as the algebraic sum of forced and natural losses.

$$Q_c = A_c l[K_{cf}(G/G^*)^{0.66} + K_{cn}((T_m - T_a)/(T_m^* - T_a^*))^{0.33}](T_m - T_a). \quad (24)$$

For large values of $G$, forced convection loss is dominant in comparison to natural convection loss, and vice versa. Considering that a part $\mu$ of incident solar energy is reflected from the tube surface, net rate of heat received at a section of external tube surface is

$$Q_m = (1 - \mu)A_r l/\Omega - Q_r - Q_c. \quad (25)$$

For economizer, evaporator and superheater, heat transfer rates $Q_{m2}$, $Q_{m4}$ and $Q_{m6}$ can be obtained in terms of respective tube wall temperatures and section lengths; these equations are listed in the Appendix.

Heat transfer from external tube surface to coolant is due to conduction (in radial direction) through tube wall and due to forced convection from inner tube surface to fluid. For a fully developed single-phase tubulent flow, convective heat transfer is computed by Dittus and Boelter relation[13]. Since hydraulic and thermodynamic property changes of compressed water and superheated steam are not significant in comparison to fluid velocity changes, heat transfer coefficient for single-phase flow is assumed to be flow-dependent only.

The regions of two-phase heat transfer can be broadly classified into wet and dry surfaces[12]. In the wet region, heat transfer coefficient is very high so that inner surface temperature is slightly above fluid saturation temperature. On the other hand, the dry or liquid deficient region has a relatively low heat transfer coefficient resulting in higher inner tube surface temperature. Heat transfer coefficient for the wet region was obtained as a function of temperature difference ($\Delta T$) and pressure from the correlations of Levy[14]. For the dry region, the data given by Bertoletti *et al.* were used[14]. The average heat transfer coefficient between inner tube surface and two-phase coolant was obtained by graphically integrating the local heat tranfer coefficient over the entire length of the evaporator. The temperature difference between the outer and inner surfaces of thick tube wall is large in comparison to that between inner tube surface and two-phase fluid. Therefore, the error due to approximation of two-phase heat transfer will not have a large bearing in the computation of heat flow $Q_4$ from external tube surface to water/steam in the evaporator.

Heat transfer rates to water/steam in the three regions are:

Economizer

$$Q_2 = A_i l_{13}(T_{m2} - T_2)/[K_{mf2}(W^*/W_1)^{0.8} + C_i] \quad (26)$$

where $C_i = r_i \ln(r_o/r_i)/k_m$.

Evaporator

$$Q_4 = A_i l_{35}(T_{m4} - T_4)/(K_{mf4} + C_i). \quad (27)$$

Superheater

$$Q_6 = A_i l_{57}(T_{m6} - T_6)/[K_{mf6}(W^*/W_1)^{0.8} + C_i]. \quad (28)$$

*Model modification*

Linearization of the steam generator model shows that

eqn (12) gives rise to an eigenvalue with a large negative real part, i.e. very fast transients are generated. To limit the time step size of integration, the differential equation (12) was made algebraic; consequently, a solution for $u_6$ must be obtained.

Average enthalpy $h_6$ of superheated steam is expressed as a function of average pressure $P_6$ and temperature $T_6$.

$$h_6 = (\alpha + \beta P_6) + (\gamma + \delta P_6) T_6 \tag{29}$$

where $\alpha$, $\beta$, $\gamma$, $\delta$ are constants of appropriate physical dimensions. Enthalpy $h_7$ of superheated steam leaving the steam generator is obtained by linear extrapolation as

$$h_7 = (h_6 - \xi_{h6} h_5)/(1 - \xi_{h6}), \; 0 < \xi_{h6} < 1 \tag{30}$$

where the averaging constant $\xi_{h6}$ is obtained from steady-state data. Similarly, $u_6$ in eqn (12) can be expressed in terms of $P_6$ and $T_6$. Therefore, a closed form solution for $T_6$ can be obtained using eqns (28)–(30) in the algebraic form of eqn (12). However, numerical calculations show that the term $\rho_5(u_6 - h_5)$ is very small and does not change appreciably under different steady-state and transient operating conditions. To simplify the expression for $T_6$, a constant value $\Phi$ is chosen for $\rho_5(u_6 - h_5)$. Therefore, the algebraic form of eqn (12) is reduced to

$$0 = W_1(h_5 - h_7) + Q_6 + A\Phi \, \mathrm{d}l_{15}/\mathrm{d}t. \tag{31}$$

Equations (28)–(31) yield a closed form solution for $T_6$.

$$T_6 = [A_i l_{57} T_{m6}/(K_{mf6}(W^*/W_1)^{0.8} + C_i) + (h_5 - \alpha - \beta P_6) W_1 /(1 - \xi_{h6}) + A\Phi \, \mathrm{d}l_{15}/\mathrm{d}t]/[A_i l_{57} /(K_{mf6}(W^*/W_1)^{0.8} + C_i) + (\gamma + \delta P_6) W_1/(1 - \xi_{h6})]. \tag{32}$$

*Steam header*

Taking the steam header as a fixed control volume, lumped parameter approximation of mass and energy conservation[15] yields

$$\mathrm{d}\rho_s/\mathrm{d}t = (nW_1 - W_v)/V_s \tag{33}$$

$$\mathrm{d}h_s/\mathrm{d}t = \left[nW_1(h_7 - h_s) + (nW_1 - W_v)\left(\frac{\partial P}{\partial \rho}\right)_{h=h_s}\right] \Big/ \left[V_s\left(\rho_s - \left(\frac{\partial P}{\partial h}\right)_{\rho=\rho_s}\right)\right]. \tag{34}$$

The header pressure $P_s$ which is obtained as a function of $\rho_s$ and $h_s$, is assumed to be equal to the pressure $P_7$ at steam generator exit (see Figs. 1 and 2).

Considering the operating mode when the turbine receives full steam, choked flow into the turbine is given as

$$W_v = K_v A_v (P_s \rho_s)^{1/2} \tag{35}$$

where normalized valve area $A_v$ is a control input, and $K_v$ is the valve constant.

*Model parameters*

The model parameters were calculated from the end point values of the plant variables, such as temperature, pressure, length, etc. for each region using the design data and physical dimensions of the steam generator tube. The steady-state model results are listed in Table 1 for four different levels of insolation under normal operating conditions.

The steady-state values of average tube wall temperatures were obtained from energy balance. Steady-state values of pressure drop and spatial average density were obtained from fluid properties and friction factors; two-phase pressure drop was calculated using the correlation of Thom[12]. The averaging constants were obtained from the steady-state values of individual plant variables at inlet, outlet and spatial average points.

## RESULTS AND DISCUSSION

The steady-state solutions of the model equations were obtained at four different levels of insolations for fixed throttle steam conditions at 510°C, $1.01 \times 10^7$ N/m$^2$ (950°F, 1465 psia). The results are listed in Table 1. With decrease in insolation, feedwater flow is reduced accordingly to maintain the throttle steam temperature; this relationship is not linear. The lengths of

Table 1. Physical dimensions and steady-state model performance

Total number os steam generator tubes = 1314.

*Dimensions of a steam generator tube*

| | | | | | |
|---|---|---|---|---|---|
| Length | 13.00 m<br>42.64 ft | I.D. | 0.00683 m<br>0.269 in. | O.D. | 0.0127 m<br>0.5 in. |

Outlet steam pressure $P_7$ { $1.01 \times 10^7$ N/m$^2$ ; 1465 psia }, temperature $T_7$ { 510°C ; 950°F }

Feedwater enthalpy at inlet $h_1$ { $1.219 \times 10^6$ J/kg ; 523.48 BTU/lbm. }

Normal air velocity $G$ { 6.7 m/sec ; 22 ft/sec }, ambient temperature $T_a$ { 15.6°C ; 60°F. }

Normal solar flux $\Omega$ { 200 kW/m$^2$ ; 19.6 BTU/(ft$^2$sec) }

Table 1. (*Contd*)

Steady-state Model Performance for Single Steam Generator Tube

| Process Variables | | | Percent Insolation | | | |
|---|---|---|---|---|---|---|
| | | | 100 | 80 | 60 | 40 |
| Water/steam flow per tube | $W_1$ | kg/s | 0.01864 | 0.01452 | 0.01041 | 0.00629 |
| | | lb/s | 0.04109 | 0.03202 | 0.02295 | 0.01388 |
| Steam flow to turbine | $W_v$ | kg/s | 24.493 | 19.081 | 13.676 | 8.270 |
| | | lb/s | 53.992 | 42.074 | 30.156 | 18.238 |
| Economizer length | $\ell_{13}$ | m | 1.190 | 1.181 | 1.171 | 1.144 |
| | | ft | 3.900 | 3.870 | 3.840 | 3.750 |
| Evaporator length | $\ell_{35}$ | m | 7.575 | 7.542 | 7.478 | 7.338 |
| | | ft | 24.850 | 24.740 | 24.530 | 24.070 |
| Superheater length | $\ell_{57}$ | m | 4.235 | 4.277 | 4.351 | 4.518 |
| | | ft | 13.890 | 14.030 | 14.270 | 14.820 |
| Economizer tube temperature | $T_{m2}$ | °C | 326.1 | 322.1 | 317.8 | 313.3 |
| | | °F | 619.0 | 611.7 | 604.1 | 596.0 |
| Evaporator tube temperature | $T_{m4}$ | °C | 340.6 | 334.7 | 328.8 | 322.9 |
| | | °F | 645.0 | 634.4 | 623.8 | 613.2 |
| Superheater tube temperature | $T_{m6}$ | °C | 453.8 | 447.7 | 440.8 | 432.2 |
| | | °F | 848.9 | 837.9 | 825.4 | 809.9 |
| Economizer heat flow | $Q_2$ | kW | 3.429 | 2.671 | 1.913 | 1.156 |
| | | BTU/s | 3.620 | 2.820 | 2.020 | 1.220 |
| Evaporator heat flow | $Q_4$ | kW | 21.749 | 16.947 | 12.144 | 7.341 |
| | | BTU/s | 22.960 | 17.890 | 12.820 | 7.750 |
| Superheater heat flow | $Q_6$ | kW | 11.501 | 8.961 | 6.423 | 3.884 |
| | | BTU/s | 12.140 | 9.460 | 6.780 | 4.10 |
| Total heat flow | $Q_2 + Q_4 + Q_6$ | kW | 36.679 | 28.579 | 20.480 | 12.381 |
| | | BTU/s | 38.720 | 30.170 | 21.620 | 13.070 |

economizer and evaporator monotonically decrease with reduction in insolation, and, therefore superheater length increases; these changes are not very significant. Due to reduction in insolation, radial heat flux decreases in each region of tube wall and results in significant changes in temperatures at external tube surface.

The nonlinear model was linearized at the steady-state operating points. The system and transfer function matrices of the linearized models were obtained (with a selected set of input and output variables) for control system design[16]; these matrices are not presented here due to sheer bulk. The system eigenvalues (which include the poles of the respective transfer functions) are listed in Table 2. Examination of the smallest (magnitude) eigenvalues shows that although the (open loop) plant is stable in the range, the dynamic response becomes monotonically slow with decrease in insolation. However, the largest (magnitude) eigenvalues could cause the plant response to be less oscillatory at lower levels of insolation. It appears that a control system designed solely on the basis of a model linearized at high load may not be adequate at low loads.

The results of the solar steam generator simulation are presented in Figs. 3–8 in the form of a series of curves

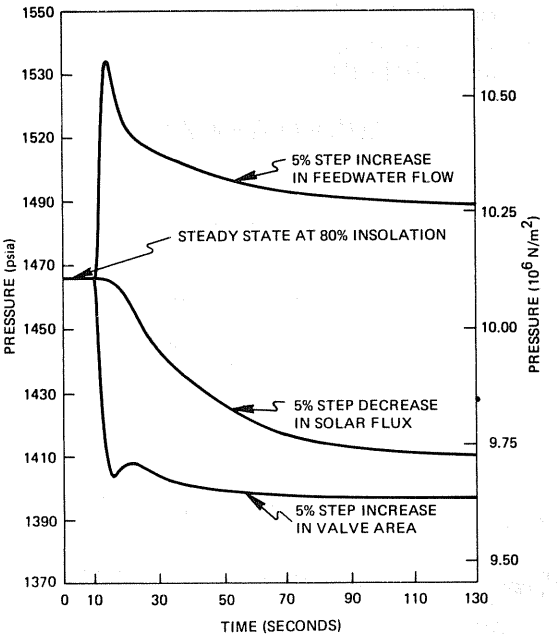


Fig. 3. Steam header pressure transients at 80 per cent insolation.

Table 2. System eigenvalues of linearized models

Dimension of the eigenvalues is $sec^{-1}$

| Percent Insolation | | | | | | | |
|---|---|---|---|---|---|---|---|
| 100 | | 80 | | 60 | | 40 | |
| Real | Imag | Real | Imag | Real | Imag | Real | Imag |
| -2.127 | +j0.815 | -1.730 | +j0.588 | -1.329 | +j0.307 | -1.150 | |
| -2.127 | -j0.815 | -1.730 | -j0.588 | -1.329 | -j0.307 | -0.691 | |
| -0.345 | +j0.460 | -0.254 | +j0.422 | -0.169 | +j0.365 | -0.092 | +j0.282 |
| -0.345 | -j0.460 | -0.254 | -j0.422 | -0.169 | -j0.365 | -0.092 | -j0.282 |
| -0.256 | | -0.204 | | -0.150 | | -0.100 | |
| -0.178 | | -0.159 | | -0.132 | | -0.088 | |
| -0.034 | | -0.026 | | -0.017 | | -0.008 | |

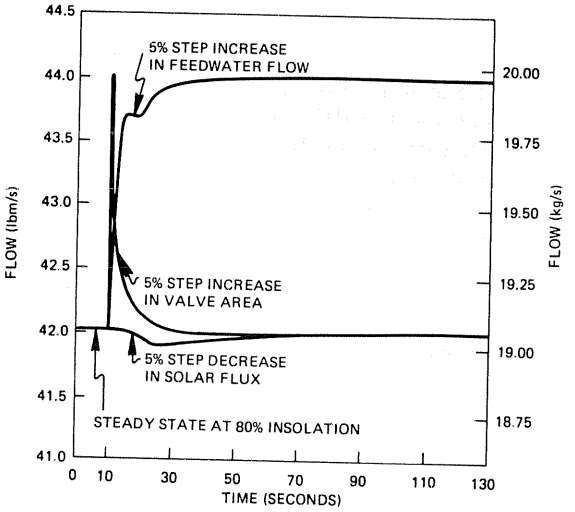


Fig. 4. Steam flow (turbine) transients at 80 per cent insolation.

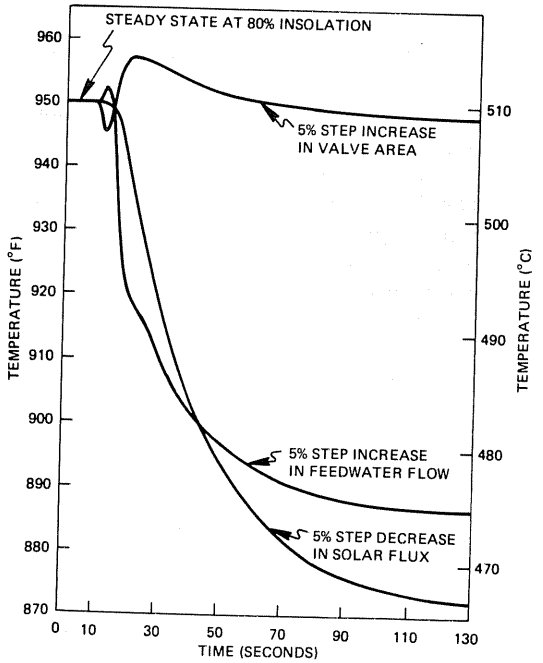


Fig. 5. Superheater outlet steam temperature transients at 80 per cent insolation.

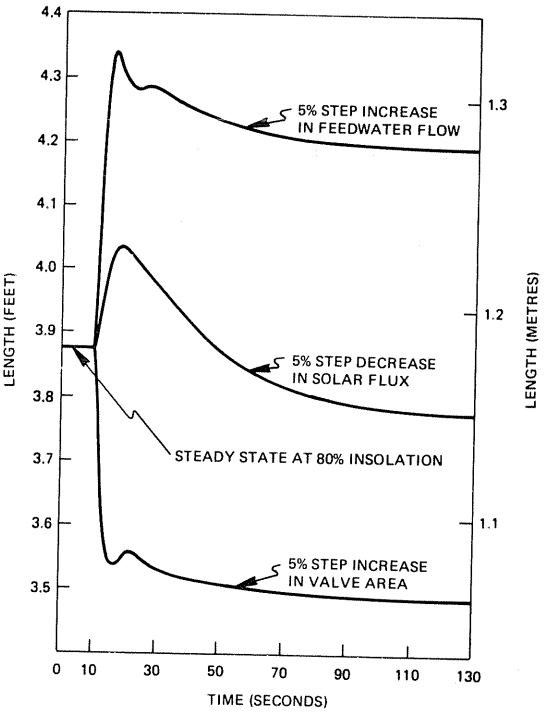


Fig. 6. Economizer length transients at 80 per cent insolation.

representing the dynamic response of 6 plant variables at 80 per cent isolation. Each figure shows three responses of a particular variable to a 5 per cent step decrease in solar flux $\Omega$, a 5 per cent step increase in feedwater flow $W_1$, and a 5 per cent step increase in turbine valve area $A_v$. In each case, the input variable under study was perturbed from its operating point keeping the other two held constant at their undisturbed value. The step disturbances were applied at time $t = 10$ sec to display the steady state condition before initiation of the disturbances. Dynamic responses were observed for a period of 130 sec.

Figure 3 shows the steam header pressure transients. A reduction in insolation decreases the stored energy in the tube wall, which, in turn, reduces the energy transfer to water/steam resulting in lower header pressure. Steam pressure starts declining after a few seconds delay and

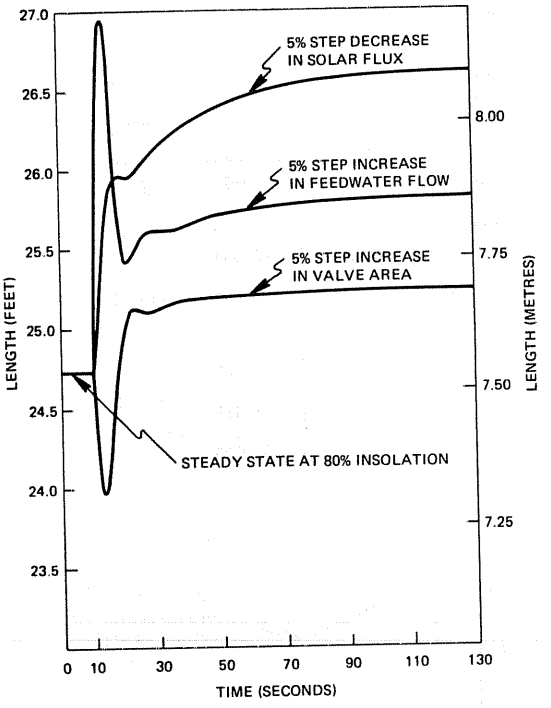


Fig. 7. Evaporator length transients at 80 per cent insolation.

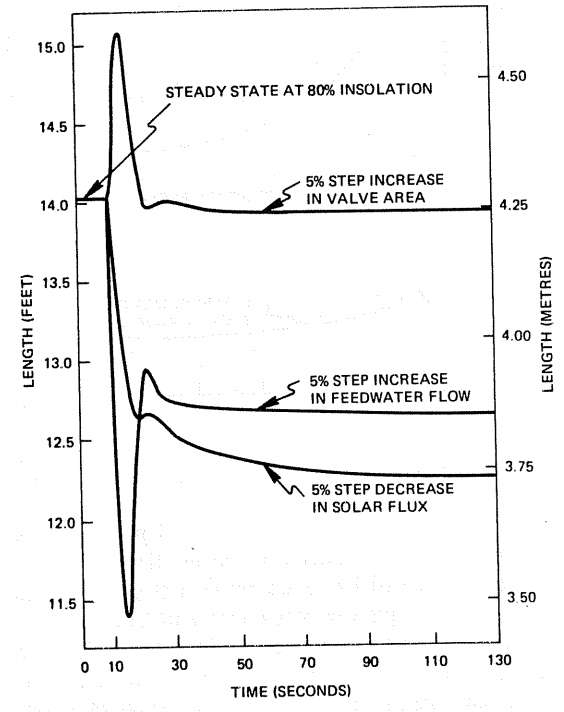


Fig. 8. Superheater length transients at 80 per cent insolation.

finally settles down in about 90 sec. An increase in feedwater flow causes an abrupt increase in header pressure resulting in a rise of steam flow into the turbine. Pressure reduces from its peak values and relaxes to steady-state in about 90 sec. An increase in value area causes an abrupt drop in header pressure. After a small oscillation, pressure stabilizes to a lower value.

Steam flow transients entering the turbine are shown in Fig. 4. A decrease in solar flux does not have a significant effect on outlet flow. After a delay of a few seconds, flow dips down a little, and essentially comes back to the original value in 1 min. An increase in feedwater flow causes a fast increase in outlet steam flow because of a stiff rise in header pressure (see Fig. 3). As header pressure drops from its peak, steam flow experiences a small dip, and then relaxes to a somewhat higher value. An increase in valve area causes an immediate rise in flow followed by a sharp drop in header pressure (see Fig. 3). Steam flow abruptly reduces from its peak and comes back to its original value in about 20 sec.

Temperature transients at the steam generator outlet are given in Fig. 5. A reduction in insolation has a delayed effect due to thermal capacitance of the tube wall. Steam temperature starts decreasing monotonically and then settles down to a lower steady-state value in about 2 min. An increase in feedwater flow results in an abrupt rise in header pressure (see Fig. 3). Since the enthalpy of steam does not respond so fast, there is an initial rise in steam temperature due to positive Joule–Thompson coefficient[17]. After this small overshoot, temperature decreases rather rapidly and then relaxes to steady-state in about 90 sec. An increase in valve area causes an immediate drop in header pressure (see Fig. 3) resulting in an initial dip in temperature followed by an overshoot of about 4°C (7°F). Then, temperature monotonically decreases and stabilizes to a lower value. The coupled thermal-hydraulic transient has a response time of about 80 sec.

Transient responses of the section lengths (i.e. economizer, evaporator and superheater) are given in Figs. 6–8. Decreased insolation reduces heat transfer to water/steam. The lengths of economizer and evaporator initially increase resulting in a decrease in superheater length and, therefore, steam temperature (see Fig. 5). Later on, economizer length stabilitizes to a lower value due to a decrease in water/steam pressure (see Fig. 3). An increase in feedwater flow results in large initial changes in the lengths of all three sections due to fast increase in pressure (Fig. 3) and, therefore, saturation temperature. After a few oscillations, phase boundaries stabilize with modest increases in economizer and evaporator lengths and a corresponding decrease in superheater length. Increased valve area causes an abrupt decrease in pressure (Fig. 3) resulting in initial decreases in economizer and evaporator lengths and a corresponding increase in superheater length. After a few small oscillations, enconomizer length stabilizes to a lower value due to a reduced water/steam pressure, and evaporator length to a higher value; superheater length comes back practically to the original value.

## CONCLUSIONS

A dynamic model of a once-through subcritical steam generator has been formulated using the concept of time-varying phase boundaries. The steam generator under consideration is of the type used in central receiver solar thermal plants. The results of this study are helpful for understanding interactive process dynamics under normal operating conditions. The model can be

used as an element in integrated solar power generation system simulation for predicting potential operational and control problems. The linearized forms of this nonlinear model are appropriate for multivariable control system design in time and/or frequency domain.

In addition to system simulation and controller design, the basic model structure formulated here can be extended to investigate the plant start-up and shutdown operations, and plant parameter sensitivity analyses.

## NOMENCLATURE

- $A$ normalized area, dimensionless
- $A_f$ tube cross-sectional area for water/steam flow, $m^2$
- $A_c$ convective area on external tube surface per unit length, m
- $A_i$ inner circumference of tube, m
- $A_r$ radiation area on external tube surface per unit length, m
- $C_m$ thermal capacity of tube material per unit length, J/(m°C)
- $f()$ functions for thermodynamic state relations
- $G$ mass flow rate of air over external tube surface, kg/sec
- $h$ specific enthalpy of water/steam, J/kg
- $K_{cf}$ heat transfer coefficient for forced convection of air, W/($m^2$°C)
- $K_{cn}$ heat transfer coefficient for natural convection of air, W/($m^2$°C)
- $K_f$ frictional pressure drop per unit length, $N/m^3$
- $K_{mf}$ inverse of heat transfer coefficient for water/steam, ($m^2$°C)/W
- $k_m$ thermal conductivity of tube material, W/(m°C)
- $l$ length of tube or tube section, m
- $n$ total number of steam generator tubes, dimensionless
- $P$ water/steam pressure, $N/m^2$
- $Q$ heat transfer rate from external tube surface to water/steam, W
- $Q_m$ net heat transfer rate from solar collector to external tube surface, W
- $r_i$ inner tube radius, m
- $r_o$ outer tube radius, m
- $T$ water/steam temperature, °C
- $T_a$ ambient temperature, °C
- $T_m$ external tube wall temperature, °C
- $T_o$ conversion constant (additive) to absolute temperature
- $t$ time, sec
- $u$ specific internal energy of water/steam, J/kg
- $V$ steam volume, $m^3$
- $W$ mass flow rate of water/steam with respect to tube wall, kg/sec
- $\alpha, \beta, \gamma, \delta$ constants for thermodynamic state relations
- $\epsilon$ emissivity of external tube surface, dimensionless
- $\lambda$ constant for gravitational pressure drop per unit length, $N/m^3$
- $\mu$ reflectivity of tube surface, dimensionless
- $\xi$ averaging constant ($0 < \xi < 1$), dimensionless
- $\rho$ density of water/steam, $kg/m^3$
- $\Phi$ constant parameter, $J/m^3$
- $\sigma$ Stefan–Boltzman constant, W/($m^2K^4$)
- $\Omega$ solar flux incident on tube surface from heliostats, W/$m^2$

*Superscripts*

- * design condition

*Subscripts*

- $s$ steam header
- $v$ turbine valve
- 1 economizer inlet
- 2 spatial average in economizer
- 3 economizer/evaporator boundary (saturated liquid)
- 4 spatial average in evaporator
- 5 evaporator/superheater boundary (saturated vapor)
- 6 spatial avarage in evaporator
- 7 superheater outlet

## REFERENCES


1. O. W. Durrant, Conceptual design of a solar advanced water/steam receiver. *Department of Energy/Sandia Laboratories Central Receiver Semiannual Meeting*, Williamsburg, VA, 11–12 September 1979.
2. K. L. Zonderman, K. F. Steffan and T. J. Connor, Dynamic computer simulation of the DoE 10MW solar thermal pilot plant. *Preprints AIAA/ASERC Conf. Solar Energy*, Paper 78–1752, Phoenix, AZ, 27–29 November 1978.
3. A. Ray and D. A. Berkowitz, Design of a practical controller for a commercial scale fossil power plant. *J. Dynamic Systems, Measurement and Control, Trans. ASME* **101**(4), 284–289 (1979).
4. D. A. Berkowitz (Ed.), *Proc. Seminar on Boiler Modeling.* The MITRE Corp., Bedford, MA (1975).
5. A. Ray and H. F. Bowman, A nonlinear dynamic model of a once-through subcritical steam generator. *J. Dynamic Systems, Measurement and Control, Trans. ASME, Series G* **98** (3), 332–339 (1976).
6. Aerospace Corp., El Segundo, CA, 10MW solar thermal pilot plant dynamic simulation. *Rep. ATR*–78(7747)–1, Vol. I (1978).
7. C. R. Easton, R. W. Hallet, A. Gronich and R. L. Gervais, Evaluation of central tower power plant. *Proc. 9th Inter-Society Energy Conversion Engineering Conf.*, San Francisco, 26–30 August 1974, pp. 271–276.
8. J. Adams, D. R. Clark, J. R. Louis and J. P. Spanbauer, Mathematical modeling once-through boiler dynamics. *IEEE Trans., Power Apparatus and Systems* **84**, 146–156 (1965).
9. H. G. Kwatny, J. P. McDonald and J. H. Spare, A nonlinear model for reheat boiler-turbine-generator systems—II. Development. *Proc. Joint Automatic Control Conf.*, St. Louis, MO, pp. 227–236 (1971).
10. R. W. McNamera, M. R. Ringham, C. C. Bramblett and L. C. Southworth, Practical simulation of an industrial fluid system with controls—The circulator auxiliaries for the Fort St. Vrain Nuclear Generating Station. *Proc. Joint Automatic Control Conf.* San Francisco, 1977, pp. 345–350.
11. A. Ray, D. A. Berkowitz and V. H. Sumaria, Nonlinear dynamic model of a fluidized bed steam generation system. *Trans. ASME, J. Engng Power* **102**, 202–208 (1980).
12. J. G. Collier, *Convective Boiling and Condensation.* McGraw-Hill, London (1972).
13. J. P. Holman, *Heat Transfer.* McGraw-Hill, New York (1976).
14. L. S. Tong, *Boiling Heat Transfer.* Wiley, New York (1965).
15. A. Ray, Approximation of fundamental equations for finite-dimensional modeling of thermo-fluid processes. *Trans. ASME, J. Engng Power* **100**, 722–723 (1978).
16. D. G. Schultz, and J. L. Melsa, *State Functions and Linear Control Systems.* McGraw-Hill, New York (1967).
17. H. B. Callen, *Thermodynamics. Wiley, New York* (1960).


## APPENDIX

*Summary of equation set constituting the model*

The seven state variables are $l_{13}$, $l_{15}$, $T_{m2}$, $T_{m4}$, $T_{m6}$, $\rho_s$ and $h_s$. The model inputs are $\Omega$, $W_1$, $h_1$ and $A_v$. Important output variables are $T_7$, $P_s$ and $W_v$.

The algebraic and differential equations constituting the model are:

$$l_{57} = l_{17} - l_{15}$$

$$l_{35} = l_{15} - l_{13}$$

$$P_7 = P_s = f(h_s, \rho_s)$$

$$P_5 = P_7 + [K_{f6}(W_1/W^*)^2 + \lambda_5]l_{57}$$

$$P_3 = P_5 + [K_{f4}(W_1/W^*)^2 + \lambda_3]l_{35}$$

$$P_1 = P_3 + [K_{f2}(W_1/W^*)^2 + \lambda_1]l_{13}$$

$$P_6 = \xi_{P6}P_5 + (1-\xi_{P6})P_7$$

$$h_5,\ T_5,\ \rho_5 = f(P_5)$$

$$h_3,\ T_3 = f(P_3)$$

$$T_4 = \xi_{T4}T_3 + (1-\xi_{T4})T_5$$

$$h_4 = \xi_{h4}h_3 + (1-\xi_{h4})h_5$$

$$u_4 = f(h_4)$$

$$h_2 = \xi_{h2}h_1 + (1-\xi_{h2})h_3$$

$$u_2,\ T_2 = f(h_2)$$

$$T_{m1} = 2T_{m2} - T_{m4}$$

$$T_{m7} = 2T_{m6} - T_{m4}$$

$$Q_{m2} = [A_r(1-\mu)\Omega - \sigma\epsilon(((T_{m1}+T_o)^4 + (T_{m4}+T_o)^4)/2 - (T_a+T_o)^4)) - A_c(K_{cf}(G/G^*)^{0.66} + K_{cn}((T_{m2}-T_a/(T_{m2}^*-T_a^*))^{0.33})(T_{m2}-T_a)]l_{13}$$

$$Q_{m4} = [A_r(1-\mu)\Omega - \sigma\epsilon((T_{m4}+T_o)^4 - (T_a+T_o)^4) - A_c(K_{cf}(G/G^*)^{0.66} + K_{cn}((T_{m4}-T_a)/(T_{m4}^*-T_a^*))^{0.33}) \times (T_{m4}-T_a)]l_{35}$$

$$Q_{m6} = [A_r(1-\mu)\Omega - \sigma\epsilon(((T_{m4}+T_o)^4 + (T_{m7}+T_o)^4/2 - (T_a+T_o)^4)) - A_c(K_{cf}(G/G^*)^{0.66} + K_{cn}((T_{m6}-T_a)/(T_{m6}^*-T_a^*))^{0.33}) \times (T_{m6}-T_a)]l_{57}$$

$$Q_2 = A_i l_{13}(T_{m2}-T_2)/[K_{mf2}(W^*/W_i)^{0.8} + C_i]$$

where

$$C_i = [r_i \ln(r_o/r_i)]/k_m$$

$$Q_4 = A_i l_{35}(T_{m4}-T_4)/(K_{mf4}+C_i)$$

$$\mathrm{d}l_{13}/\mathrm{d}t = [W_1(h_1-h_3) + Q_2]/(A_f\rho_3(u_2-h_3))$$

$$\mathrm{d}l_{15}/\mathrm{d}t = [W_1(h_3-h_5) + Q_4 + A_f\rho_3(u_4-h_3)\,\mathrm{d}l_{13}/\mathrm{d}t]/(A_f\rho_5(u_4-h_5))$$

$$T_6 = [A_i l_{57}T_{m6}/(K_{mf6}(W^*/W_1)^{0.8} + C_i) + (h_5 - \alpha - \beta P_6)W_1/(1-\xi_{h6}) + A_f\Phi\,\mathrm{d}l_{15}/\mathrm{d}t]/[A_i l_{57}/(K_{mf6}(W^*/W_1)^{0.8} + C_i) + (\gamma + \delta P_6)W_1/(1-\xi_{h6})]$$

$$Q_6 = A_i l_{57}(T_{m6}-T_6)/(K_{mf6}(W^*/W_1)^{0.8} + C_i)$$

$$h_6 = (\alpha + \beta P_6) + (\gamma + \delta P_6)T_6$$

$$h_7 = (h_6 - \xi_{h6}h_5)/(1-\xi_{h6})$$

$$T_7 = f(h_7, P_7)$$

$$\mathrm{d}T_{m2}/\mathrm{d}t = (Q_{m2}-Q_2)/(C_m l_{13}) + ((T_{m4}-T_{m2})/l_{13})\mathrm{d}l_{13}/\mathrm{d}t$$

$$\mathrm{d}T_{m4}/\mathrm{d}t = (Q_{m4}-Q_4)/(C_m l_{35})$$

$$\mathrm{d}T_{m6}/\mathrm{d}t = (Q_{m6}-Q_6)/(C_m l_{57}) + ((T_{m6}-T_{m4})/l_{57})\mathrm{d}l_{15}/\mathrm{d}t$$

$$W = K_v A_v(P_s\rho_s)^{1/2}$$

$$\mathrm{d}\rho_s/\mathrm{d}t = (nW_1 - W_v)/V_s$$

$$\mathrm{d}h_s/\mathrm{d}t = \left[W_1(h_7-h_s) + (nW_1 - W_v)\left(\frac{\partial P}{\partial \rho}\right)_{h=h_s}\right] \Big/ \left[V_s\left(\rho_s - \left(\frac{\partial P}{\partial h}\right)_{\rho=\rho_s}\right)\right]$$

$$T_s = f(h_s, \rho_s).$$